Clean Energy Science and Technology 2024, 2(3), 121.
https://doi.org/10.18686/cest.v2i3.121

Article

Prussian blue nanoparticles: Synthesis and experimental evaluation as electrocatalyst for hydrogen evolution reaction

Mukhtiar Ahmed[1,2,3,*], Irfan Ali Soomro[4], Kishore Chand[3], Yang Yang[1]

[1] State Key Laboratory of Mesoscience and Engineering, Institute of Process Engineering, Chinese Academy of Sciences, Beijing 100190, China
[2] University of Chinese Academy of Sciences, Beijing 100190, China
[3] Key Laboratory of Superlight Material and Surface Technology, Ministry of Education, College of Materials Science and Chemical Engineering, Harbin Engineering University, Harbin 150001, China
[4] College of Chemical Engineering, Beijing University of Chemical Technology, Beijing 100190, China
*** Corresponding author:** Mukhtiar Ahmed, ahmedmukhtiar461@gmail.com

CITATION

Ahmed M, Soomro IA, Chand K, Yang Y. Prussian blue nanoparticles: Synthesis and experimental evaluation as electrocatalyst for hydrogen evolution reaction. Clean Energy Science and Technology. 2024; 2(3): 121. https://doi.org/10.18686/cest.v2i3.121

ARTICLE INFO

Received: 15 January 2024
Accepted: 10 September 2024
Available online: 26 September 2024

Abstract: The reliance on fossil fuels has led to numerous environmental challenges, highlighting the urgent need for alternative energy sources that minimize contamination and promote eco-friendliness. In this context, hydrogen (H_2) emerges as a promising fuel due to its zero-carbon emissions. Within various methods for H_2 production, electrochemical water splitting (EWS) stands out as a viable approach. Traditionally, noble metals, such as platinum and iridium, have been employed as electrocatalysts to efficiently facilitate the hydrogen evolution reaction (HER) in desired electrolytes (such as alkaline). Recently, research has focused on the use of Prussian blue (PB) as an innovative electrocatalyst material for EWS. Herein, we developed PB-based electrocatalysts for HER in an alkaline medium. The electrocatalyst comprising PB combined with phosphorus exhibited impressive electrochemical properties, achieving a minimal overpotential of 103 mV at a current density of 10 mA/cm^2 and maintaining durability over 20 h, along with extended electrochemical performance. This material composition has considerable promise as a potential option for energy conversion systems, which can aid future sustainability initiatives.

Keywords: Prussian blue; electrocatalysis; energy conversion; HER

1. Introduction

Researchers are investigating hydrogen (H_2) as a potential energy replacement for conventional fossil fuels due to its high energy density and clean, sustainable qualities. As the world seeks sustainable alternatives to fossil fuels, the efficient production of H_2 through hydrogen evolution reaction (HER) presents a promising pathway for clean energy solutions [1–3]. When H_2 is utilized, it produces water as a by-product, which is environmentally friendly and free of pollutants. Nevertheless, other technical challenges related to the production, storage, and transportation of H_2 still require solutions [4–6]. Electrochemical water splitting (EWS) is an important technology for producing hydrogen. It involves two reactions: HER and oxygen evolution reaction (OER). In this study, we focused on HER [7,8]. Higher overpotentials usually accelerate these reactions due to their inherently sluggish kinetics. Currently, precious metals, such as platinum, are valued for their significance in HER [9]. However, their high cost and restricted supply restrict their widespread commercial use worldwide [10]. Therefore, creating adaptable electrocatalysts with high efficiency, low cost, and a long lifetime is essential for putting integrated energy systems into practice in the future [9]. The presence of hydrogen on an

electrocatalyst's surface has a small effect on HER in slightly alkaline conditions. Additionally, the detachment of water prevents the adsorption of hydroxyl ions (OH). The dissociation of H_2O is a crucial step in HER under alkaline conditions [11,12].

For the purpose of HER, a number of transition metal compounds, including oxides, sulfides, and phosphides, have been presented as a promising alternative to electrocatalysts based on noble metals [13–16]. In the frameworks of energy conversion and energy storage, transition metal oxides play a significant role in energy conversion and storage. Some examples of these frameworks are lithium-ion batteries, sodium-ion batteries, hybrid supercapacitors, and water-splitting applications [17,18]. Simultaneously, Prussian blue (PB) and its analogues are intriguing materials for energy storage, as well as conversion, because of their distinctive features. PB is a material produced by the oxidation of Fe(II) cyanide salts. Its chemical formula is $Fe^{III}_4[Fe^{II}(CN)_6]_3$ [19]. PB was originally produced through an unforeseen reaction involving cochineal, iron sulfide, and cyanide, with the intention of producing a red dye [20]. By replacing the iron component with different transition metals, including nickel, cobalt, and manganese, numerous variations of PB have been discovered. These compounds are categorized as a subset of the metal-organic framework because they possess diverse metallic elements and three-dimensional extended structures. The materials demonstrate high stability, excellent reversibility, and cost-effectiveness, making them appealing options for a variety of applications [21,22]. PB has demonstrated promise as a cathode material in sodium-ion batteries and potassium-ion batteries in the field of energy storage. Its electrochemical characteristics, including high capacity and cycling stability, make it a feasible choice for future battery technologies. Prussian white, a PB analogue, has been studied for its potential application in supercapacitors due to its high capacitance and consistent cycling behavior [23]. Such phenomena make them ideal for situations where efficient energy storage and discharge are essential. PB-based materials have been widely researched as electrocatalysts for energy conversion as well, particularly for OER and HER. Their effective catalytic performance and minimal overpotentials make them beneficial for water-splitting applications, which is crucial for renewable H_2 production [24,25].

Furthermore, the characteristics of sodium dihydrogen phosphate and selenium in PB are favorable and provide effective remedies to initial challenges, including enhancing electrochemical stability, and improving catalytic performance [26]. PB-based composites are generally produced using a suitable mixing method. Additionally, PB-selenide/phosphates with a crystalline structure are more intriguing due to their superior conductive properties and capacity for rapid electron transport compared with materials recently disclosed for energy conversion and electrochemical applications [27].

In this article, we comprehensively discuss the structural characteristics of PB and introduce its applications in energy conversion. This study demonstrated a PB-derived electrocatalyst for HER. The desired materials were prepared through the wet-chemical method and analyzed through different physicochemical characterizations, which were X-ray diffractometry (XRD), scanning electron microscopy (SEM), and energy-dispersive X-ray spectroscopy (EDS), to confirm their crystallinity, morphology, and elemental presence, respectively. The method of our synthesis and

electrochemical analysis based on PB has rarely been reported yet. Therefore, our prepared material and its electrochemical results are efficient.

2. Materials and experimental methodology

2.1. Materials and reagents

The composite materials and reagents utilized in this research included polyvinylpyrrolidone (C_6H_9NO) and pure selenium powder, both sourced from Sinopharm Chemical Reagents Co., Ltd. Additionally, potassium ferrocyanide ($K_4Fe(CN)_6$), dilute hydrochloric acid (HCl), and sodium dihydrogen phosphate (NaH_2PO_4) were obtained from Tianjin Yaohua Chemical Reagents Co. Ltd. A 1 × 1 cm piece of nickel foam was also employed in the experiments. The equipment underwent a thorough washing process using deionized water to ensure cleanliness for the studies. The selenium powder had a purity level of 97%. The NaH_2PO_4 reagent was acquired from a chemical reagent supplier in Tianjin, China. All chemicals were added to the reaction without any additional treatment to maintain consistent and reliable experimental conditions.

2.2. Preparation of materials

Synthesis of PB nanocubes: Following the procedures described in our previous research, we synthesized PB nanocubes using the following reagents: 60 g C_6H_9NO, 3.3 g $K_4Fe(CN)_6$, 10.02 g HCl, and 1200 mL distilled water. As illustrated in **Figure 1**, the resulting combined solution was maintained at a temperature of 80 °C for 24 h, with continuous magnetic stirring for 30 min. The mixture was then dried in an oven for the required duration. This process yielded a sample of PB with a highly uniform cubic morphology.

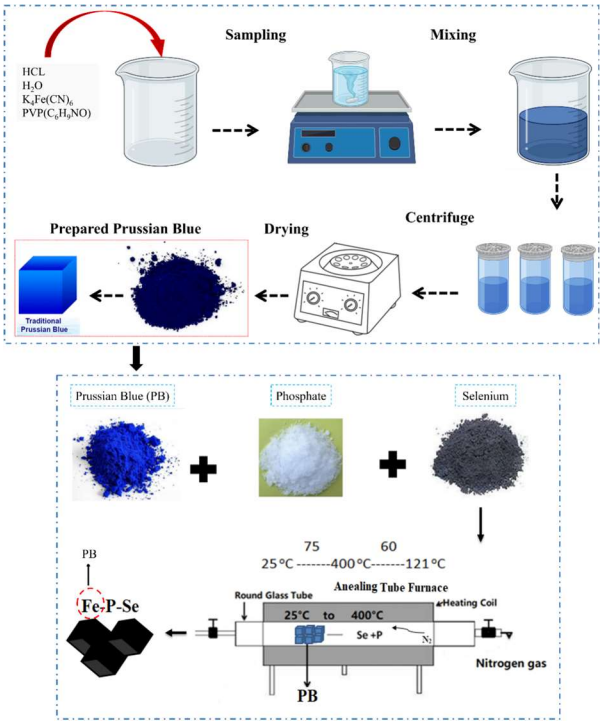

Figure 1. Diagrammatic representation of process for making PB and its derivatives.

Preparation of composites: As shown in **Figure 1**, the synthesized PB was subsequently combined with phosphorus (P) and selenium (Se) individually, as well as with both P and Se elements, to create three distinct composites, which were PB-P, PB-Se, and PB-P-Se, through an annealing process. For the PB-Se-P composite, 0.25 g of NaH_2PO_4 and 0.2 g of Se were placed upstream, while 0.42 g of PB was positioned downstream, in a tube furnace to ensure optimal contact with the gas stream. The annealing tube was heated to 400 °C for 3 h in a nitrogen atmosphere, with a heating rate of 5 °C/min. After cooling at room temperature, PB-Se, PB-P, and PB-Se-P composites were successfully obtained.

2.3. Characterizations of samples

The crystalline structure and purity of the samples were analyzed using a Rigaku TTR X-ray diffractometer with specific settings. XRD analysis was conducted at a current density of 45 mA, acceleration voltage of 45 kV, and wavelength of 0.15406 nm for Cu Kα radiation. SEM was performed using a JEOL JSM-6480A system operating at 20 kV to investigate the morphology of the obtained samples. An EDS detection device attached to the SEM instrument was utilized to conduct the elemental analysis of the materials. These characterization techniques allowed for a comprehensive understanding of the structural, compositional, and morphological properties of the synthesized PB and its composites, providing valuable insights into their potential applications.

3. Results and discussion

3.1. Chemical and crystalline structure of PB

Spectroscopic investigations confirmed that PB is composed of iron(III) cyanide, represented as $Fe^{3+}[Fe^{2+}(CN)_6]_3$. In this structure, iron(III) atoms are bonded to nitrogen (N) atoms, while iron(II) atoms are bonded to carbon (C) atoms. PB can be synthesized through the chemical combination of iron(III) ions (Fe^{3+}) and hexacyanoferrate ions ($Fe^{2+}[Fe(CN)_6]_4$), depending on the oxidation states of the Fe atoms involved in the reaction. Upon mixing these components, a dark blue colloid forms immediately. In contrast, mixed solutions containing both iron(II) ions (Fe^{2+}) and hexacyanoferrate ions, which share the same oxidation state, tend to remain stable without precipitating. The crystalline structure of PB was first investigated by Keggin and Miles in 1936, they utilized powder diffraction patterns to analyse its properties. Studies have contributed significantly to understanding the composition and structural characteristics of PB. Ludi and colleagues advanced the understanding of PB's crystalline structure through detailed electron and neutron diffraction studies of single crystals [28]. In this structure, Fe^{3+} and Fe^{2+} ions are arranged alternately within a face-centered cubic lattice, forming the fundamental cubic framework of PB. Fe^{3+} ions are octahedrally coordinated by nitrogen atoms, while Fe^{2+} ions are coordinated by carbon atoms. As illustrated in **Figure 2**, a quarter of $Fe(CN)_6$ groups are absent, resulting in an average of only 18 cyanide ions instead of the expected 24, along with three iron atoms. This deficiency in cyanide groups contributes to the unique properties of PB

and highlights the importance of precise structural analysis in understanding its composition and behavior.

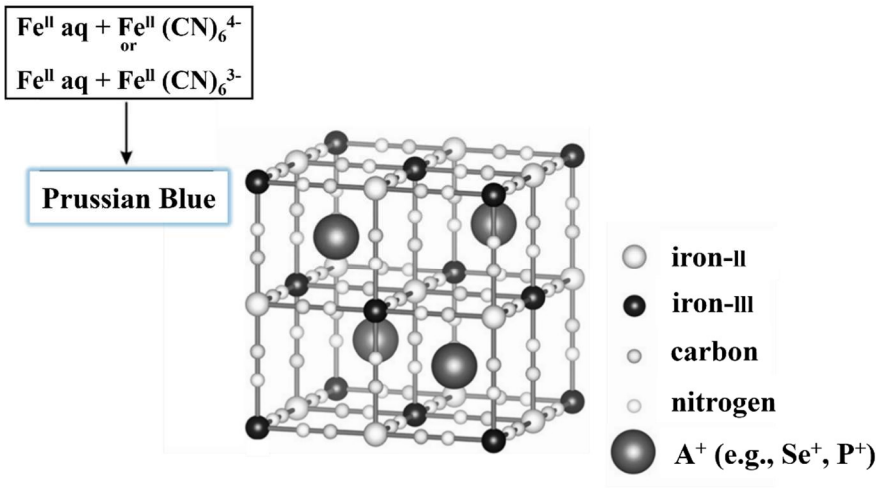

Figure 2. Unit cell of PB, with all sites occupied.

PB nanoparticles offer several structural benefits that enhance their effectiveness in energy conversion applications. Their face-centered cubic structure provides high stability, which is crucial for maintaining performance during operation. The nano-sized particles possess a large surface area, facilitating significant electrode-electrolyte interactions for improving overall efficiency. Moreover, the porous structure of these nanoparticles facilitates effective ion transport, hence augmenting their activity. The elevated redox activity of PB nanoparticles is a significant benefit, since they possess many redox active sites for facilitating fast electron transfer during charge and discharge cycles. This attribute enhances their superior electrochemical stability throughout cycling, guaranteeing a consistent performance over time. Furthermore, PB has intrinsic catalytic characteristics that facilitate hydrogen evolution reaction, making it a significant material for H_2 production.

3.2. Morphological and elemental analysis

The elemental composition of the synthesized materials was assessed using EDS, which can effectively identify the various elements present in a sample. The EDS analysis revealed distinct peaks corresponding to PB, as well as additional peaks for phosphorus and selenium. A typical EDS spectrum is displayed as a plot of X-ray counts versus energy (in keV), where each energy peak correlates to a specific element within the sample. While the peaks in the spectrum are generally sharp and well-resolved, the presence of multiple elements can result in numerous overlapping peaks. Notably, the iron component of PB shows significant Kα and Kβ peaks, which are indicative of its concentration and oxidation state. This is illustrated in **Figure 3**. Overall, the EDS analysis provided critical insights into the elemental composition of the synthesized materials, confirming the successful incorporation of the components, which is essential for understanding the materials' properties and potential applications.

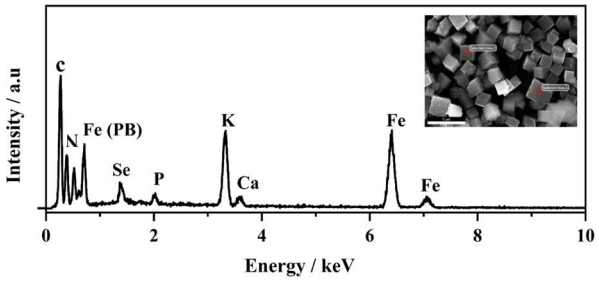

Figure 3. EDS analysis of PB.

In addition to elemental analysis, we employed SEM to examine the morphological features of the PB nanoparticles. The SEM images clearly revealed a distinct cubic structure characteristic of PB, highlighting the uniformity and consistency of the nanoparticles. This morphological insight is crucial, as the unique cubic shape contributes significantly to the materials' properties, such as its surface area and reactivity. Understanding these morphological characteristics enhances the knowledge of how PB nanoparticles interact in various environments, which is vital for their potential applications. The cubic structure not only facilitates efficient packing in fixed-bed reactors but also promotes effective electron transfer and ion diffusion, making PB nanoparticles particularly suitable for energy conversion and storage applications. Overall, SEM analysis provides valuable information that supports the exploration of PB nanoparticles in diverse fields, including catalysis and electrochemical systems. The morphology of the annealed products was examined using SEM, revealing that the structure of the pure PB was both uniform and cubic in shape. This consistent cubic morphology is significant for a variety of applications, particularly in catalysis for energy conversion processes. The uniform structure enhances the material's surface area and active sites, facilitating more efficient interactions during catalytic reactions. These characteristics are crucial for optimizing performance in energy-related applications, such as hydrogen evolution and battery technologies. The findings are illustrated in **Figures 4(a–d)**, which visually demonstrated the cubic structure of the PB nanoparticles and highlighted their potential efficacy in advancing energy conversion technology.

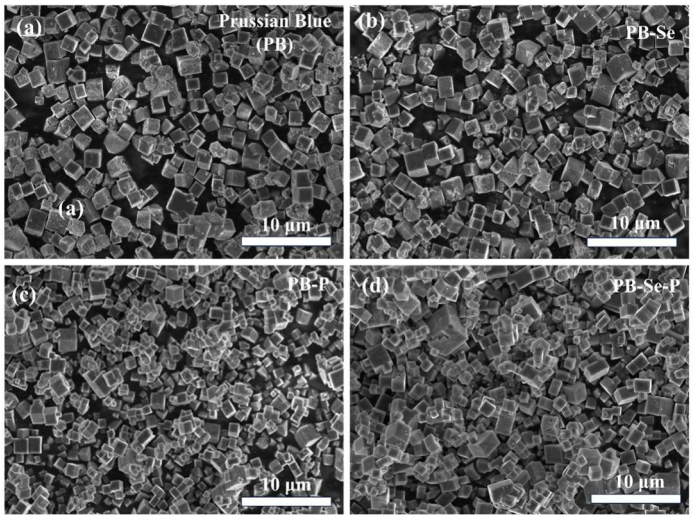

Figure 4. SEM images of PB and its composites.

To investigate the morphological details of the PB-P composite, we conducted transmission electron microscopy (TEM) analysis. The TEM images, presented in **Figure 5**, showcase the PB-P composite at various magnifications ranging from 1 μm to 200 nm. These high-resolution images provided valuable insights into the surface characteristics of the material at the nanoscale level. The TEM analysis clearly demonstrated that the PB-P composite maintained a well-defined cubic structure, consistent with the previously reported morphology of pure PB. This consistency in the cubic shape across different compositions was significant, as it suggested that the addition of P did not significantly alter the central structure of PB. The preservation of the cubic morphology is crucial for maintaining the desirable properties associated with PB, such as high surface area and efficient ion transport, which are essential for its performance in energy conversion and storage applications. The TEM images at higher magnification (200 nm) reveal intricate details of the cubic structure, highlighting its uniformity and the absence of significant defects or irregularities. This level of structural control is essential for ensuring consistent performance and reproducibility in practical applications. Overall, the TEM analysis complemented the SEM findings and provided a comprehensive understanding of the morphological characteristics of the PB-P composite, further supporting its potential for use in advanced energy technologies. The well-defined cubic structure of the PB-P composite promotes effective electrochemical performance. The uniform and consistent morphology enhances the material's properties, making it suitable for various energy-related applications [29].

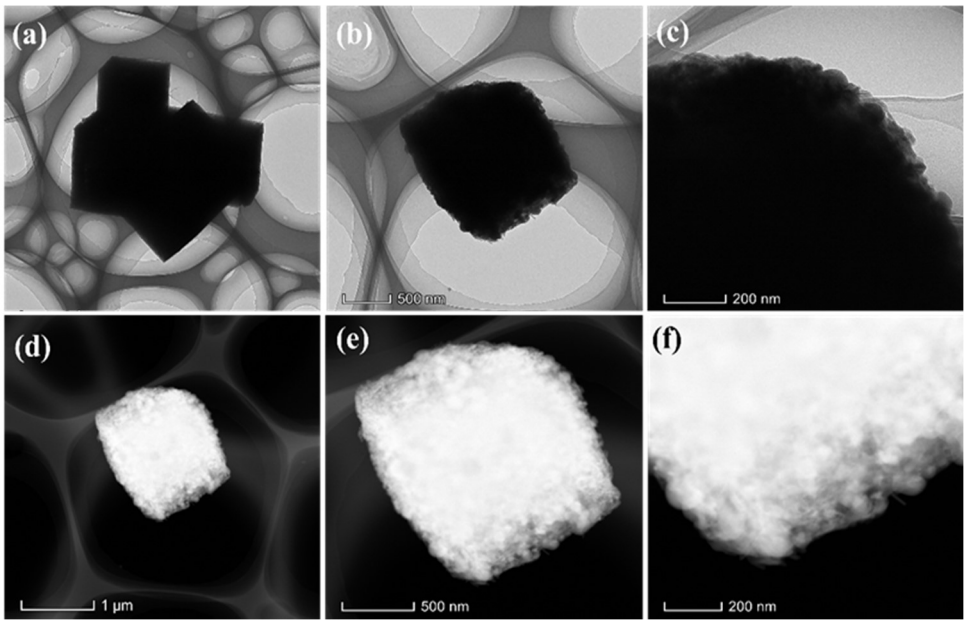

Figure 5. TEM images of PB-P at various magnifications.

3.3. Crystallographic analysis of PB

The crystallographic analysis of the as-prepared PB was conducted using XRD, with the resulting spectra displayed in **Figure 6**. The XRD patterns revealed distinct peaks at two theta values of 17.1°, 24.6°, 30.4°, 35.2°, 39.5°, and 43.4°, which corresponded to crystallographic planes (200), (220), (222), (400), (420), and (422),

respectively. These well-defined peaks indicated that the PB material was successfully synthesized without significant impurities in its crystal structure. The presence of a pure crystal structure is crucial, as it enhances a material's properties, particularly its electrical conductivity. A purer PB composition can lead to improved charge transport, which is essential for optimizing reaction kinetics during HER. Consequently, the favorable crystallographic characteristics of the synthesized PB not only confirmed its successful preparation but also suggested its potential for enhanced performance in electrochemical systems.

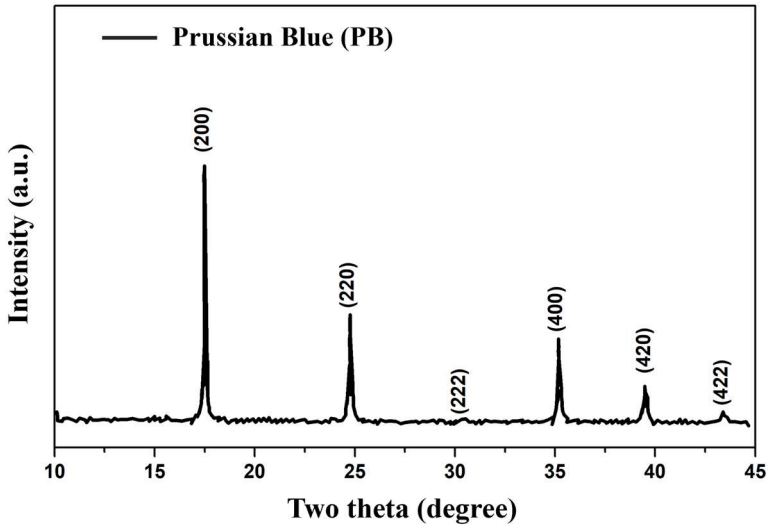

Figure 6. XRD patterns of as-prepared PB.

3.4. Electrochemical analysis

The electrocatalytic performance of PB for HER was investigated in an alkaline environment. Initially, to assess the HER efficiency of PB, we employed linear sweep voltammetry (LSV) in a 1.0 M KOH solution. This method allowed for a detailed evaluation of the catalysts' activity by measuring the current response at varying applied potentials. The results obtained from the LSV analysis provide critical insights into the catalytic capabilities of PB, enabling us to determine its effectiveness in facilitating HER under alkaline conditions [30]. The polarization curves obtained from the LSV measurements for various electrocatalysts are presented in **Figure 7**. Notably, PB-P exhibited a remarkably low overpotential of 103 mV at a current density of 10 mA/cm^2, while the other electrocatalysts displayed higher overpotential values. This low overpotential, combined with the higher current density observed for PB-P, indicated its superior efficiency for HER in an alkaline medium, as illustrated in **Figure 7a**. Additionally, the Tafel slope is a critical parameter for evaluating the reaction kinetics associated with electrochemical water splitting. We calculated the Tafel slope values for the prepared electrocatalysts using the Tafel equation, as shown in **Figure 7b**. The Tafel slope provided insights into the rate-determining step of HER and allowed us to compare the reaction kinetics of different catalysts. A lower Tafel slope value typically suggests faster reaction kinetics, further supporting the enhanced electrocatalytic performance of PB-P in facilitating HER [31,32].

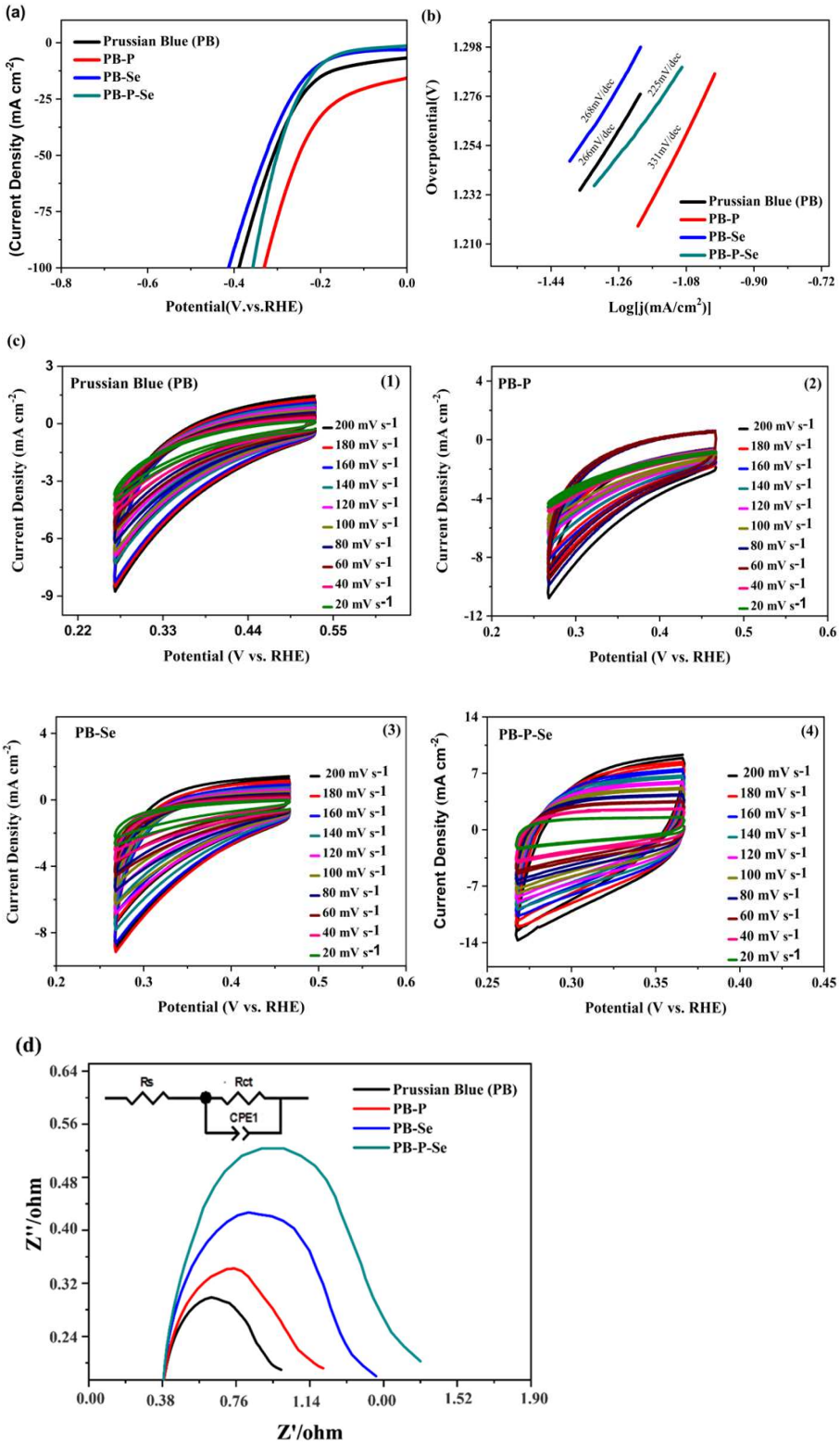

Figure 7. Electrocatalytic behavior of PB and its composites for HER in KOH: **(a)** LSV curves; **(b)** Tafel slopes; **(c)** CV curves at varying scan rates, and **(d)** EIS.

Using the Nernst equation, the potential of a reversible hydrogen electrode (RHE) can be derived from the silver/silver-chloride (Ag/AgCl) reference potential. The relevant equations and parameters are outlined below [33].

The Nernst equation is given by Equation (1):

$$E = E^o \frac{nF}{RT} \ \mathrm{In}Q \tag{1}$$

Importantly, the Nernst equation is a fundamental relationship in electrochemistry, which allows for the calculation of the electrode potential (E) of a reaction under non-standard conditions. This potential is influenced by several key variables, which are the standard electrode potential (E^o), the number of moles of electrons transferred in the reaction (n), Faraday's constant (F), the universal gas constant (R), the temperature in Kelvin (T), and the reaction quotient (Q), which represents the ratio of the concentrations of products to reactants at a given moment in time.

The potential of the RHE can be expressed as Equation (2):

$$E_{RHE} = E_{Ag/AgCl} + 0.059\, pH + E^o_{Ag/AgCl} \tag{2}$$

where,

$$E_{Ag/AgCl} = 0.2412 \tag{3}$$

The overpotential (η) is determined by subtracting the onset thermodynamic potential of the water-splitting system, which is 0 V for HER, as in Equation (4):

$$\eta = E_{RHE} - 0V \tag{4}$$

To analyze the relationship between overpotential and current density, the Tafel equation is utilized, as in Equation (5):

$$\eta = b \cdot \log j + a \tag{5}$$

In the above Tafel equation, the variables are defined as follows: η indicates the overpotential required to surpass equilibrium, reflecting the energy barrier. The Tafel slope (b) relates overpotential to the logarithm of current density, with a steeper slope indicating higher activation energy. Current density (j) measures electric current per unit area of the electrode, which is directly linked to the reaction rate. The Tafel intercept (a) represents the overpotential at a current density of 1 A/cm^2, serving as a performance reference. Together, these parameters are crucial for optimizing electrochemical processes in various applications [34].

Cyclic voltammograms (CVs) were obtained in the potential range of 0.27–0.37 V to investigate the electrochemical properties of PB and its composites. The CV tests were conducted at various scan rates, as illustrated in **Figures 7c(1–4)**, to enhance interpretation and facilitate comparison of results. The measurements were performed in a 1.0 M KOH solution, carefully selected to ensure that the potential window excluded Faradaic processes. The scan rates employed ranged from 20 to 200 mV/s, allowing for a comprehensive analysis of the electrochemical behavior. Importantly, charge transfer kinetics play a vital role in determining the performance of an electrocatalyst, as they influence the efficiency of electron transfer between the electrode and the electrolyte. By examining the shape and position of the oxidation and reduction peaks in the CVs, researchers can gain insights into the reversibility of electrochemical reactions and the overall catalytic activity. Understanding these kinetics is vital for optimizing electrocatalyst design, leading to improved performance in electrochemical applications [35].

Electrical impedance spectroscopy (EIS) was conducted to gain deeper insights into the interfacial reactions and electrode kinetics of PB and its composites, as

illustrated in **Figure 7d**. A charge transfer resistance (R_{ct}) value of 50 Ω for PB-P was calculated. The low R_{ct} values, combined with a high effective surface area, indicated that PB can facilitate rapid charge transfer and offer additional active sites during HER. As a result, PB demonstrated exceptional electrocatalytic performance, making it a promising candidate for efficient energy conversion applications. However, the stability of an electrocatalyst for practical use is an important factor [36]. Therefore, we analyzed our prepared material (PB-P) for stability through a chronopotentiometry test at 10 mA/cm^2. Interestingly, in the graph of potential vs. current density, it was seen that the PB-P electrocatalyst showed a very stable nature without any major changes, as shown in **Figure 8**. Furthermore, this material was compared with those from other recent research studies on HER, as demonstrated in **Table 1** [37–46].

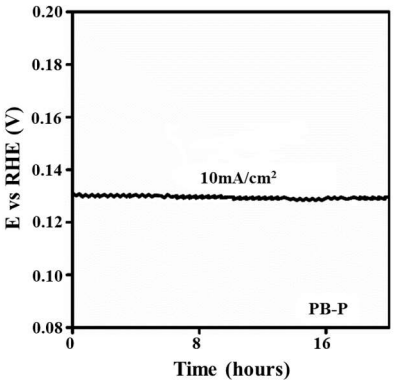

Figure 8. Chronopotentiometry analysis for stability of PB-P electrocatalyst.

Table 1. Comparative analysis of PB-P electrocatalyst with those in literature.

Electrocatalyst	Overpotential (mV)	Current density	Tafel slope	Electrolyte
$CoNi_2S_4$–CNFs	228	20	42.1	1.0 M KOH
rGO@SN-$CoNi_2S_4$	142.6	10	61	1 mol·L^{-1} KOH
CoS_2/BCN	292	10	121	1.0 M KOH
Co_9S_8@MoS_2/CNFs	190	10	110	1.0 M KOH
NS/rGO-Co_4	150	10	92	1.0 M KOH
$CoNi_2S_4$/g–C_3N_4@NF	160	10	90.76	1.0 M KOH
CoFeS/CNT	~150	10	67	0.5 M H_2SO_4
FeP/NCNT	195	100	59	0.5 M H_2SO_4
Mo_2C/CNT	152	10	55.2	0.1 M $HClO_4$
$NiMoN_x$/C	170	20	24	0.1 M $HClO_4$

4. Conclusion

In this study, PB-based materials were synthesized using the one-pot synthesis method and characterized to evaluate their physicochemical properties. SEM analysis provided insights into their morphology, while EDS analysis confirmed the elemental composition. XRD analysis demonstrated the crystalline structure of the PB-based electrocatalysts. The electrochemical performances of the as-prepared PB, PB-P, PB-Se, and PB-P-Se were assessed in a 1.0 M KOH solution for HER. PB-P electrocatalyst

achieved a low overpotential of 103 mV at a current density of 10 mA/cm² and exhibited remarkable stability, maintaining performance for 20 h under the same conditions. The electrochemical findings highlight the promise of PB-based materials as efficient electrocatalysts for energy conversion systems to facilitate the development of a hydrogen economy and aid the transition to a sustainable society. The comprehensive characterizations and electrochemical analyses provided valuable insights into the relationship between structure and performance for guiding future optimization of PB-based materials for enhanced efficiency and durability in energy conversion applications.

Author contributions: Conceptualization, MA and IAS; methodology, MA; software, MA; validation, MA and KC; formal analysis, MA; investigation, MA and IAS; resources, MA; data curation, MA and YY; writing—original draft preparation, MA and IAS; writing—review and editing, MA and YY; visualization, MA and YY; supervision, MA; project administration, MA; funding acquisition, MA. All authors have read and agreed to the published version of the manuscript.

Funding: The authors acknowledge financial supports from the National Natural Science Foundation of China (NSFC 51402065 and 51603053) and the Natural Science Foundation of Heilongjiang Province (LH2019E025). We also express gratitude and thanks to the National Key Research and Development Program of China (Grant No. 2016YFF0102601), as well as to the Strategic Priority Research Program of the Institute of Process Engineering, Chinese Academy of Sciences, for providing resources.

Conflict of interest: The authors declare that they have no known competing financial interests or personal relationships that could have appeared to influence the work reported in this paper.

References

1. Chen L, Ren J, Yuan Z. Design strategies of phosphorus-containing catalysts for photocatalytic, photoelectrochemical and electrocatalytic water splitting. Green Chemistry. 2022; 24(2): 713-747. doi: 10.1039/D1GC03768D
2. Aftab U, Tahira A, Samo AH, et al. Mixed CoS_2@Co_3O_4 composite material: An efficient nonprecious electrocatalyst for hydrogen evolution reaction. International Journal of Hydrogen Energy. 2020; 45(27): 13805-13813. doi: 10.1016/j.ijhydene.2020.03.131
3. Hanan A, Shu D, Aftab U, et al. Co_2FeO_4@ rGO composite: Towards trifunctional water splitting in alkaline media. International Journal of Hydrogen Energy. 2022; 47(80): 33919-33937. doi: 10.1016/j.ijhydene.2022.07.269
4. Weng C, Lv X, Ren J, et al. Engineering Gas–Solid–Liquid Triple-Phase Interfaces for Electrochemical Energy Conversion Reactions. Electrochemical Energy Reviews. 2022; 5(Suppl 1): 19. doi: 10.1007/s41918-022-00133-x
5. Laghari AJ, Aftab U, Tahira A, et al. MgO as promoter for electrocatalytic activities of Co_3O_4–MgO composite via abundant oxygen vacancies and Co^{2+} ions towards oxygen evolution reaction. International Journal of Hydrogen Energy. 2023; 48(34): 12672-12682. doi: 10.1016/j.ijhydene.2022.04.169
6. Ali Bhutto Y, Pandey AK, Saidur R, et al. Electrical and thermal performance assessment of photovoltaic thermal system integrated with organic phase change material. E3S Web of Conferences. 2024; 488: 01007. doi: 10.1051/e3sconf/202448801007
7. Hanan A, Lakhan MN, Shu D, et al. An efficient and durable bifunctional electrocatalyst based on PdO and Co_2FeO_4 for HER and OER. International Journal of Hydrogen Energy. 2023; 48(51): 19494-19508. doi: 10.1016/j.ijhydene.2023.02.049

8. Aftab U, Solangi MY, Tahira A, et al. An advanced PdNPs@MoS_2 nanocomposite for efficient oxygen evolution reaction in alkaline media. RSC Advances. 2023; 13(46): 32413-32423. doi: 10.1039/D3RA04738E
9. Raja Sulaiman RR, Hanan A, Wong WY, et al. Structurally modified MXenes-based catalysts for application in hydrogen evolution reaction: A review. Catalysts. 2022; 12(12): 1576. doi: 10.3390/catal12121576
10. Ibupoto ZH, Tahira A, Shah AA, et al. $NiCo_2O_4$ nanostructures loaded onto pencil graphite rod: An advanced composite material for oxygen evolution reaction. International Journal of Hydrogen Energy. 2022; 47(10): 6650-6665. doi: 10.1016/j.ijhydene.2021.12.024
11. Hao LP, Hanan A, Walvekar R, et al. Synergistic Integration of MXene and Metal-Organic Frameworks for Enhanced Electrocatalytic Hydrogen Evolution in an Alkaline Environment. Catalysts. 2023; 13(5): 802. doi: 10.3390/catal13050802
12. Zuo Y, Bellani S, Saleh G, et al. Ru–Cu Nanoheterostructures for Efficient Hydrogen Evolution Reaction in Alkaline Water Electrolyzers. Journal of the American Chemical Society. 2023; 145(39): 21419-21431. doi: 10.1021/jacs.3c06726
13. Ren J, Chen L, Wang H, et al. Water electrolysis for hydrogen production: From hybrid systems to self-powered/catalyzed devices. Energy & Environmental Science. 2024; 17(1): 49-113. doi: 10.1039/D3EE02467A
14. Hanan A, Ahmed M, Lakhan MN, et al. Novel rGO@Fe_3O_4 nanostructures: An active electrocatalyst for hydrogen evolution reaction in alkaline media. Journal of the Indian Chemical Society. 2022; 99(5): 100442. doi: 10.1016/j.jics.2022.100442
15. Qureshi RA, Hanan A, Abro MI, et al. Facile eggplant assisted mixed metal oxide nanostructures: A promising electrocatalyst for water oxidation in alkaline media. Materials Today Sustainability. 2023; 23: 100446. doi: 10.1016/j.mtsust.2023.100446
16. Balu S, Hanan A, Venkatesvaran H, et al. Recent Progress in Surface-Defect Engineering Strategies for Electrocatalysts toward Electrochemical CO_2 Reduction: A Review. Catalysts. 2023; 13(2): 393. doi: 10.3390/catal13020393
17. Ren J, Chen L, Wang H, Yuan Z. High-entropy alloys in electrocatalysis: From fundamentals to applications. Chemical Society Reviews. 2023; 52(23): 8319-8373. doi: 10.1039/D3CS00557G
18. Shaheen I, Ali I, Bibi F, et al. Integrating 1D/2D nanostructure based on Ni–Co-oxalate for energy storage applications. Ceramics International. 2023; 50(7A): 10789-10796. doi: 10.1016/j.ceramint.2023.12.394
19. Chen J, Wei L, Mahmood A, et al. Prussian blue, its analogues and their derived materials for electrochemical energy storage and conversion. Energy Storage Materials. 2020; 25: 585-612. doi: 10.1016/j.ensm.2019.09.024
20. Guichard C, Le Hô AS, Williams H. Prussian Blue: Chemistry, Commerce, and Colour in Eighteenth-Century Paris. Art History. 2023; 46(1): 154-186. doi: 10.1111/1467-8365.12695
21. Zhao D, Lu Y, Ma D. Effects of Structure and Constituent of Prussian Blue Analogs on Their Application in Oxygen Evolution Reaction. Molecules. 2020; 25(10): 2304. doi: 10.3390/molecules25102304
22. Bhutto YA, Pandey AK, Saidur R, et al. Analyzing the thermal potential of binary 2D (h-BN/Gr) nanoparticles enhanced lauric acid phase change material for photovoltaic thermal system application. Journal of Energy Storage. 2023; 73: 109116. doi: 10.1016/j.est.2023.109116
23. Fayaz M, Lai W, Li J, et al. Prussian blue analogues and their derived materials for electrochemical energy storage: Promises and Challenges. Materials Research Bulletin. 2024; 170: 112593. doi: 10.1016/j.materresbull.2023.112593
24. Samo A, Aftab U, Cao D, et al. Schematic synthesis of cobalt-oxide (Co_3O_4) supported cobalt-sulfide (CoS) composite for oxygen evolution reaction. Digest Journal of Nanomaterials & Biostructures (DJNB). 2022; 17(1): 109. doi: 10.15251/djnb.2022.171.109
25. Solangi MY, Aftab U, Tahira A, et al. In-situ growth of nonstoichiometric $CrO_{0.87}$ and Co_3O_4 hybrid system for the enhanced electrocatalytic water splitting in alkaline media. International Journal of Hydrogen Energy. 2023; 48(93): 36439-36451. doi: 10.1016/j.ijhydene.2023.06.059
26. Jia N, Huang B, Chen L, et al. A simple non-enzymatic hydrogen peroxide sensor using gold nanoparticles-graphene-chitosan modified electrode. Sensors and Actuators B: Chemical. 2014; 195: 165-170. doi: 10.1016/j.snb.2014.01.043
27. Lu Y, Saroja APVK, Wei R, Xu Y. Engineering metal selenides for sodium-and potassium-ion batteries. Cell Reports Physical Science. 2021; 2(9): 100555. doi: 10.1016/j.xcrp.2021.100555
28. Buser HJ, Schwarzenbach D, Petter W, Ludi A. The crystal structure of Prussian blue: $Fe_4[Fe(CN)_6]_3 \cdot xH_2O$. Inorganic Chemistry. 1977; 16(11): 2704-2710. doi: 10.1021/ic50177a008
29. Hussain I, Ahmad M, Kewate OJ, et al. V-MXenes for energy storage/conversion applications. ChemSusChem. 2024; 17(15): e202400283. doi: 10.1002/cssc.202400283

30. Hanan A, Laghari AJ, Solangi MY, et al. CdO/Co_3O_4 nanocomposite as an efficient electrocatalyst for oxygen evolution reaction in alkaline media. International Journal of Engineering Science Technologies. 2022; 6(1): 1-10. doi: 10.29121/IJOEST.v6.i1.2022.259
31. Hanan A, Lakhan MN, Solangi MY, et al. MXene based electrocatalyst: CoS_2@$Ti_3C_2T_x$ composite for hydrogen evolution reaction in alkaline media. Materials Today Sustainability. 2023; 24: 100585. doi: 10.1016/j.mtsust.2023.100585
32. Ahmed M, Hanan A, Lakhan MN, et al. One-pot synthesis of crystalline structure: Nickel-iron phosphide and selenide for hydrogen production in alkaline water splitting. Journal of Electrochemical Science and Engineering. 2023; 13(3): 575-588. doi: 10.5599/jese.1721
33. Ahmed M, Lakhan MN, Shar AH, et al. Electrochemical performance of grown layer of $Ni(OH)_2$ on nickel foam and treatment with phosphide and selenide for efficient water splitting. Journal of the Indian Chemical Society. 2022; 99(1): 100281. doi: 10.1016/j.jics.2021.100281
34. Solangi MY, Samo AH, Laghari AJ, et al. MnO_2@Co_3O_4 nanocomposite based electrocatalyst for effective oxygen evolution reaction. Sukkur IBA Journal of Emerging Technologies. 2022; 5(1): 32-40. doi: 10.30537/sjet.v5i1.958
35. Lakhan MN, Hanan A, Wang Y, et al. Recent Progress on Nickel-and Iron-Based Metallic Organic Frameworks for Oxygen Evolution Reaction: A Review. Langmuir. 2024; 40(5): 2465-2486. doi: 10.1021/acs.langmuir.3c03558
36. Hanan A, Lakhan MN, Bibi F, et al. MOFs coupled transition metals, graphene, and MXenes: Emerging electrocatalysts for hydrogen evolution reaction. Chemical Engineering Journal. 2024; 482: 148776. doi: 10.1016/j.cej.2024.148776
37. Hanan A. Magnesium doped cobalt-oxide composite for active oxygen evolution reaction. Journal of Applied and Emerging Sciences. 2021; 11(2): 210-216. doi: 10.36785/JAES.112519
38. Deng BL, Guo LP, Lu Y, et al. Sulfur–nitrogen co-doped graphene supported cobalt–nickel sulfide rGO@SN-$CoNi_2S_4$ as highly efficient bifunctional catalysts for hydrogen/oxygen evolution reactions. Rare Metals. 2022; 41(3): 911-920. doi: 10.1007/s12598-021-01828-8
39. Borthakur P, Boruah PK, Das MR, et al. CoS_2 Nanoparticles Supported on rGO, g-C_3N_4, BCN, MoS_2, and WS_2 Two-Dimensional Nanosheets with Excellent Electrocatalytic Performance for Overall Water Splitting: Electrochemical Studies and DFT Calculations. ACS Applied Energy Materials. 2021; 4(2): 1269-1285. doi: 10.1021/acsaem.0c02509
40. Zhu H, Zhang J, Yanzhang R, et al. When Cubic Cobalt Sulfide Meets Layered Molybdenum Disulfide: A Core–Shell System Toward Synergetic Electrocatalytic Water Splitting. Advanced Materials. 2015; 27(32): 4752-4759. doi: 10.1002/adma.201501969
41. Wang N, Li L, Zhao D, et al. Graphene Composites with Cobalt Sulfide: Efficient Trifunctional Electrocatalysts for Oxygen Reversible Catalysis and Hydrogen Production in the Same Electrolyte. Small. 2017; 13(33): 1701025. doi: 10.1002/smll.201701025
42. Zahra R, Pervaiz E, Baig MM, et al. Three-dimensional hierarchical flowers-like cobalt-nickel sulfide constructed on graphitic carbon nitride: Bifunctional non-noble electrocatalyst for overall water splitting. Electrochimica Acta. 2022; 418: 140346. doi: 10.1016/j.electacta.2022.140346
43. Huang L, Wu H, Liu H, et al. Phosphorous doped cobalt-iron sulfide/carbon nanotube as active and robust electrocatalysts for water splitting. Electrochimica Acta. 2019; 318: 892-900. doi: 10.1016/j.electacta.2019.06.096Get
44. Liu Q, Pu Z, Asiri AM, et al. Nitrogen-doped carbon nanotube supported iron phosphide nanocomposites for highly active electrocatalysis of the hydrogen evolution reaction. Electrochimica Acta. 2014; 149: 324-329. doi: 10.1016/j.electacta.2014.10.105
45. Chen WF, Wang CH, Sasaki K, et al. Highly active and durable nanostructured molybdenum carbide electrocatalysts for hydrogen production. Energy & Environmental Science. 2013; 6(3): 943-951. doi: 10.1039/C2EE23891H
46. Chen WF, Sasaki K, Ma C, et al. Hydrogen-Evolution Catalysts Based on Non-Noble Metal Nickel–Molybdenum Nitride Nanosheets. Angewandte Chemie International Edition. 2012; 51(25): 6131-6135. doi: 10.1002/anie.201200699